Experimental Characterization of the Vane Heat Flux Under Pulsating Trailing-Edge Blowing

J. Saavedra
Maurice J. Zucrow Laboratories
Purdue University,
West Lafayette, IN 47907
e-mail: saavedra@purdue.edu

G. Paniagua
Maurice J. Zucrow Laboratories
Purdue University,
West Lafayette, IN 47907

B. H. Saracoglu
von Karman Institute for Fluid Dynamics,
Rhode Saint Genèse,
Brussels 1640, Belgium

The steady improvement of aircraft engine performance has led toward more compact engine cores with increased structural loads. Compact single-stage high-pressure turbines allow high power extraction, operating in the low supersonic range. The shock waves formed at the airfoil trailing edge contribute substantially to turbine losses, mainly due to the shock-boundary layer interactions as well as high-frequency forces on the rotor. We propose to control the vane trailing edge shock interaction with the downstream rotor, using a pulsating vane-trailing-edge-coolant at the rotor passing frequency. A linear cascade of transonic vanes was investigated at different Mach numbers, ranging from subsonic to supersonic regimes (0.8, 1.1) at two engine representative Reynolds numbers (4×10^6 and 6×10^6). The steady and unsteady heat flux was retrieved using thin-film two-layered gauges. The complexity of the tests required the development of an original heat transfer postprocessing approach. In a single test, monitoring the heat flux data and the wall temperature we obtained the adiabatic wall temperature and the convective heat transfer coefficient. The right-running trailing edge shock wave impacts on the neighboring vane suction side. The impact of the shock wave on the boundary layer creates a separation bubble, which is very sensitive to the intensity and angle of the shock wave. Increasing the coolant blowing rate induces the shock to be less oblique, moving the separation bubble upstream. A similar effect is caused by the pulsations of the coolant
[DOI: 10.1115/1.4035211]

1 Introduction

The modern aero-engine combustors operate nearly at adiabatic flame temperatures, well above the melting temperature of super alloys, and elevated pressure ratios to deliver the power demand with high efficiency. Consequently, first turbine stages are exposed to extreme flow conditions. The high pressure and temperature flow expands to supersonic velocities over high pressure turbine passages. Complex shock systems appear at the vane trailing edge and impact on the neighboring airfoils (Fig. 1(*a*)). The interaction of the shock waves with the boundary layer over the neighboring vane and the downstream row results in significant efficiency reduction and high cycle fatigue problems [1]. Denton and Xu [2,3] described the shock loses as 1/3 of the total loss in transonic turbines.

The thermal loading on the high pressure turbine stages severely impacts on the life-cycle of the airfoils. In order to maintain the structural integrity of the components, the turbine airfoils are heavily cooled. Over the entire volume of the nozzle guide vanes, the trailing edge region is a vulnerable section of the airfoil as the material thickness is the smallest. Therefore, to avoid melting, the majority of the coolant is ejected through a slot at the trailing edge.

The flow field around the trailing edge section comprises peculiar structures (Fig. 1(*b*)). The streams coming from each side of the trailing edge expands over Prandtl–Meyer expansion fan and immediately detaches from the airfoil. The separated shear layers join at the confluence region and form a compression ramp where the shock waves are generated. Upstream of this region, enclosed by the separated shear layer, low momentum flow recirculates at the base region where the coolant is ejected. Several researchers [4–8] have investigated the interactions between the coolant purge and trailing edge flow structures. It has been demonstrated that the coolant regime strongly modulates the pressure at the base region, shock waves, and consequently the losses in transonic airfoils.

Sieverding et al. [9] experimentally tested the relation between the flow acceleration conditions and the base pressure level over the trailing edge of a flat plate with streamwise pressure gradient. Consequently, an empirical correlation was constructed depicting the changes in the base pressure level with the downstream pressure; providing quantification of the base pressure loss for a variety of turbine cascades. Sieverding [10] examined the effect of the coolant density and purge rate on the variation of base pressure of a transonic model. The experimental evidences pointed an optional purge rate to augment the base pressure and thus alleviate the losses. Particle image velocimetry (PIV) measurements performed by Raffel and Kost [6] showed that the trailing edge flow field and the compression waves were altered at certain coolant mass flow rates. Saracoglu et al. numerically simulated the influence of a wide range of steady cooling rates on the trailing edge flow of a flat plate exposed to supersonic stream [7]. The results depicted that there exists an optimum blowing rate increasing the base pressure, reducing the trailing edge shock intensity, and consequently reducing the losses. The experimental and numerical investigation over a transonic cascade showed that the pulsating cooling modulates the shock structures and the trailing edge unsteadiness [11].

The heat transfer problem in the high pressure turbine cascades has been extensively studied by several research groups [12–15]. The adiabatic wall temperature (T_{aw}) was introduced to uniquely quantify the convective heat transfer process [16]. Multiple methodologies have been proposed to calculate the heat transfer coefficient from a series of experiments over the same aerodynamical configuration with different wall temperature conditions [17,18].

This study experimentally investigates heat transfer characteristics of a transonic cascade with continuous and pulsating trailing edge cooling. The novelty of this research relies in the application of an innovative way to process the heat transfer measurements to attain the adiabatic heat transfer coefficient. The quantification of the thermal effects of the pulsating trailing edge cooling was based on thin films wall temperature measurements, taking

Contributed by the International Gas Turbine Institute (IGTI) of ASME for publication in the Journal of Turbomachinery. Manuscript received September 18, 2016; final manuscript received September 29, 2016; published online February 1, 2017. Editor: Kenneth Hall.

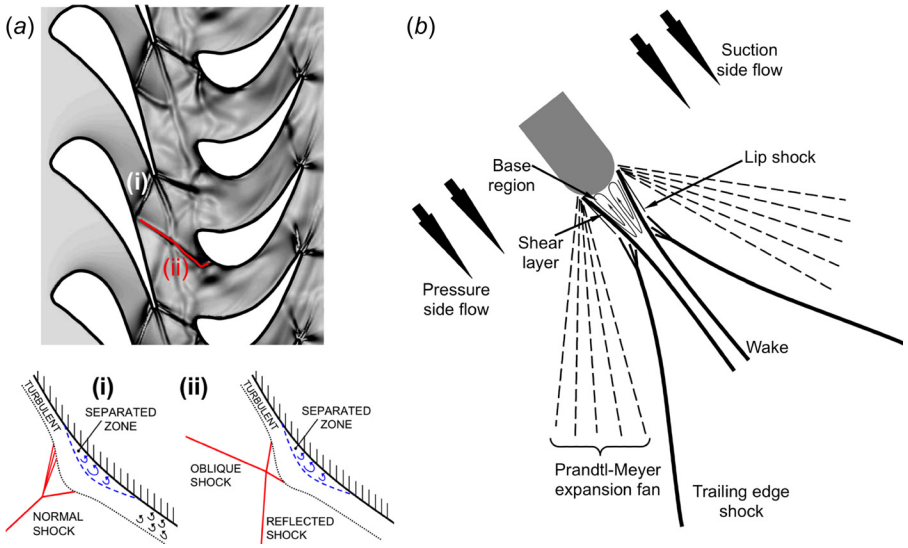

Fig. 1 (*a*) Shock interactions over a transonic turbine stage and (*b*) zoom on the expansion and compression trailing edge waves

advantage of the adiabatic wall temperature definition. Through the application of the criteria described here, the extraction of the heat transfer characteristics on the airfoils is performed based on a single experiment. Finally, the proposed methodology applied on the current experimental apparatus depicts the modulation of the trailing edge shock waves by the unsteady trailing edge cooling.

2 Measurement Techniques

The inlet total pressure and temperature fluctuations were recorded with a Pitot probe and a K-type microthermocouple placed one chord upstream of the model leading edge.

Surface temperature measurements were performed on the suction side contoured top wall of the test section. The assessment of the wall temperature variation was accomplished by variable resistance thermometers deposited over a thin film layer. The thin film gauges consist of a nickel resistive element glued into a polyamide flexible substrate Figs. 2(*a*) and 2(*b*).

The variation on the metal temperature results in changes on its electric resistance according to the law

$$R = R_0(1 + \alpha_T\ (T - T_0)\ ) \tag{1}$$

where R_0 is the resistance at the reference temperature (T_0) and α_T is the temperature coefficient, which correlates the resistivity with the material temperature. Each gauge was connected to the fourth leg of a Wheatstone bridge, which was fed with constant current. The gauges were individually calibrated in order to determine the temperature coefficient.

The Fig. 2(*c*) sketches the investigated airfoil, including the actual location, 130 mm and 45 mm upstream of the trailing edge. The so-called upstream gauge is located at the geometrical throat, where the trailing edge shock wave from the neighboring airfoil should impinge. Thanks to the high conductivity of the Nickel and its large resistivity, the thin films results extremely sensitive to thermal variations, thus allowing high frequency temperature measurements.

The sensing element is deposited over a low conductivity layer of polyamide of 200 μm, which is glued to the metallic airfoil. Due to the thickness of the polyamide, a double layer postprocessor is required to trace the transient heat flux variation. The entire unsteady surface-temperature data acquisition was done at sampling frequency of 1 MHz.

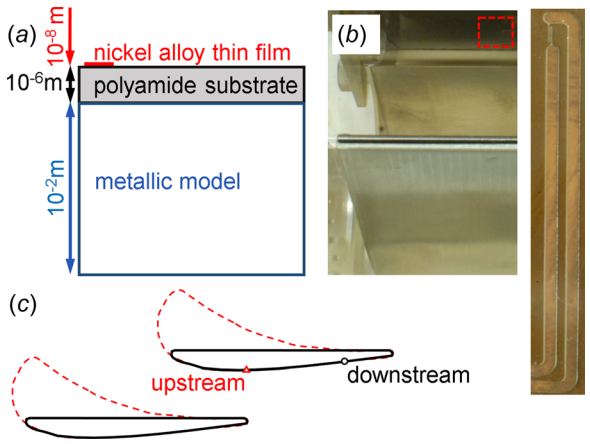

Fig. 2 (*a*) Double layered domain, (*b*) airfoil trailing edge and thin film example, and (*c*) vane and gauge locations

3 Experimental Methodology of Convective Heat Flux in Transients

3.1 One-Dimensional Numerical Heat Flux Approach to Solve Conduction. The classical data reduction technique used for double-layered thin-film gauges is based on the resolution of the 1D unsteady heat conduction as given in the following equation:

$$\frac{1}{\alpha}\frac{\partial T}{\partial t} = \frac{\partial^2 T}{\partial^2 x}\ \frac{1}{\alpha}\frac{\partial T}{\partial t} = \frac{\partial^2 T}{\partial^2 x} \tag{2}$$

Several techniques have been employed for thin film gauge data processing, consisting on analog circuits [19,20], fast Fourier transform techniques [21], or the numerical solution of the unsteady heat conduction equation in the gauge substrate [22]. These methods rely commonly on two assumptions: the substrate is considered as semi-infinite during the test duration; and the heat conduction occurs in a monodimensional manner. The data reduction technique consists on solving the 1D unsteady heat conduction equation imposing as the top boundary condition the temperature history provided by the thin film gauges in the airfoil surface. In this approach, the bottom boundary condition is tracked in time and used as rear condition for the numerical solver.

Due to the existence of several substrates, an additional boundary condition must be imposed at the interface between each substrate, the heat flux continuity

$$-k_1\left[\frac{\partial T}{\partial x}\right]_{x=L^-} = -k_2\left[\frac{\partial T}{\partial x}\right]_{x=L^+} \tag{3}$$

Various tactics have been proposed to account for the presence of multilayered substrates [19,23,24], considering the domain depicted in the Fig. 3 left. The materials properties are listed in Table 1.

A Crank–Nicholson numerical discretization is employed to solve the 1D unsteady heat conduction equation. It provides the temperature field in the substrate at every time step and, subsequently, the wall heat flux at the gauge location. The Crank–Nicolson method [25] is first-order accurate in space and second-order in time. It is based on the trapezoidal rule, giving second-order convergence in time. For example, in one dimension, if the partial differential equation is $(\partial u/\partial t) = F(u, x, t, (\partial u/\partial x), (\partial^2 u/\partial x^2))$, this method is a combination of the Forward Euler method at n, and the backward Euler method for $n+1$

$$\frac{u_i^{n+1} - u_i^n}{\Delta t} = \frac{1}{2}\left[F_i^{n+1}\left(u, x, t, \frac{\partial u}{\partial x}, \frac{\partial^2 u}{\partial x^2}\right) + F_i^{n+1}\left(u, x, t, \frac{\partial u}{\partial x}, \frac{\partial^2 u}{\partial x^2}\right)\right] \tag{4}$$

It is spatially implicit, hence, in order to solve the system of equations, the whole system must be solved at once due to its nonlinearity nature. Based on its time evolution it can be written as an implicit Runge–Kutta method enhancing its numerical stability. The discretization characteristic of such a scheme is presented on the Fig. 3 right.

This method is implemented in a numerical solver in order to postprocess the wall temperature data. The tool is verified against the surface convection analytical solution from Incropera and coworkers [26] (Fig. 4)

$$\frac{T(x,t) - T_i}{T_\infty - T_i} = \operatorname{erfc}\left(\frac{x}{2\sqrt{\alpha t}}\right) - \left[\exp\left(\frac{hx}{k} + \frac{h^2\alpha t}{k^2}\right)\right]\left[\operatorname{erfc}\left(\frac{x}{2\sqrt{\alpha t}} + \frac{h\sqrt{\alpha t}}{k}\right)\right] \tag{5}$$

3.2 Adiabatic Convective Heat Transfer Coefficient. Given the substrate temporal evolution, the local convective heat transfer coefficient can be directly estimated. Prior studies proposed several approaches to compute the heat transfer coefficient in the quest for more accurate heat flux description. Moffat [16] and Popp et al. [27] introduced a method based on the definition of the adiabatic wall temperature. It consists of acquiring the wall temperature value, which results on null heat transfer between the fluid and the solid. This method was developed based on the realization of several experiments at the same aerothermal conditions, modifying only the test article wall temperature. As depicted in Fig. 5, the heat transfer is represented against the wall temperature.

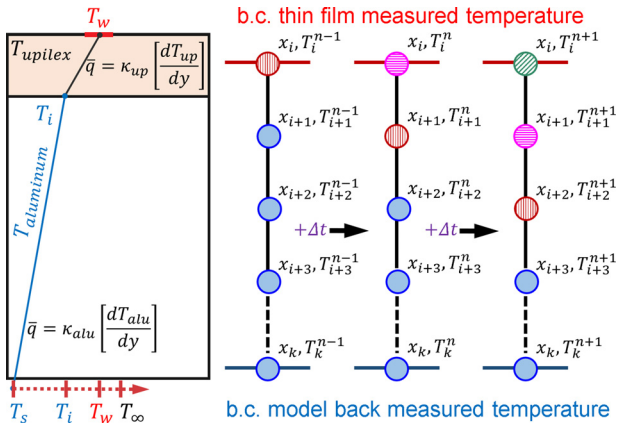

Fig. 3 (Left) Heat conduction across multilayered substrates, (Right) Heat flux data reduction based on 1D semi-infinite assumption with a Crank Nicolson scheme

Table 1 Material properties

	Upilex	Aluminum	Unit
Thickness	0.15	>40	mm
Density	1470	2700	kg/m^3
Heat capacity	1130	897	J/(kg K)
Thermal conductivity	0.288	180	W/(m K)
Thermal diffusivity	1.73×10^{-7}	7.43×10^{-5}	m^2/s

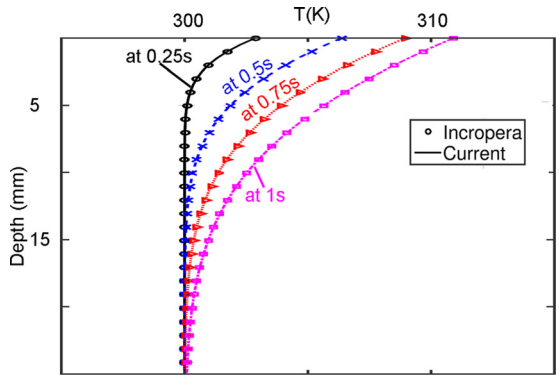

Fig. 4 Validation of the code developed to solve the transient heat transfer

As discussed by Lavagnoli et al. [28], the heat flux could be exponentially related with the adiabatic wall temperature and the temperature difference, Eq. (6), albeit considering experimental window restrictions and the sensitivity of this method, the uncertainty results higher than the expected accuracy

$$q = h_{\text{aw}}\left(\frac{T_w}{T_{\text{aw}}}\right)^n (T_{\text{aw}} - T_w) \tag{6}$$

The process could be similarly described making use of the Newton cooling law Eq. (7), being the adiabatic wall temperature Refs. [29] and [30]

$$q = h_{\text{aw}}(T_{\text{aw}} - T_w) \tag{7}$$

Based on the equation proposed by Pinilla et al. [18], the time-averaged heat transfer rate can be expressed based on two different terms

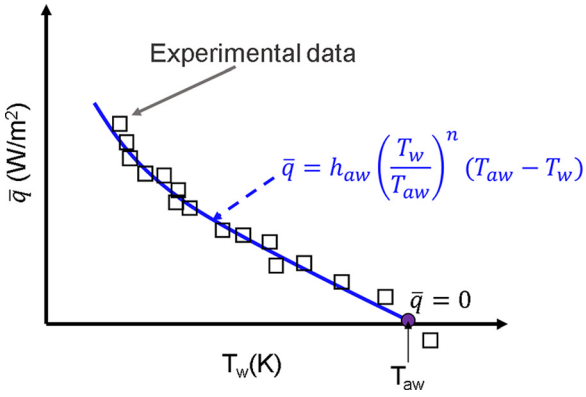

Fig. 5 Heat transfer coefficient computation based on heat flux data and adiabatic wall temperature definition

$$\overline{q} + q' = (\overline{h_{aw}} - h'_{aw})(T_{aw} + T'_{aw} - T_w) \quad (8)$$

The steady influence based on the time-mean heat transfer coefficient and adiabatic wall temperature, and the unsteady contribution arising from the fluctuations in these parameters. In the regions where the amplitude of the oscillations is small, the unsteady heat flux term results negligible, and the heat flux can be accurately described making use of time-mean quantities

$$\overline{q} = \overline{h_{aw}}\,(\overline{T_{aw}} - T_w) + \overline{h'_{haw} T'_{aw}} \quad (9)$$

Independently of the unsteady terms contribution on the heat flux characterization, Eq. (9), the convective heat transfer coefficient remains unaltered as depicted in Fig. 6.

3.3 Application for Short Transient Testing. Figure 7 displays the evolution of total temperature and pressure recorded upstream of the test section the experiment. Based on the total pressure and temperature evolution, the test duration is determined by the total pressure plateau and the total temperature steady behavior. The maximum oscillation of the freestream temperature based on a root-mean-square deviation is limited to 2%, in order to avoid the effect of sudden wall temperature variations on the heat flux reduction process.

Applying the described methodology, the heat flux is represented against the wall temperature. Then making use of the adiabatic wall temperature definition, the adiabatic heat transfer coefficient is extracted.

The inverted C shape of the heat flux versus wall temperature (Fig. 8 right) representation is due to the decay of the freestream temperature by the end of the experiment. The variations of the absolute temperature lead to sudden variation on the wall temperature. If the wall temperature is suddenly reduced and immediately raised up, it is reflected into a minor loop on the $\overline{q}$ versus T_w representation (Fig. 8 right). Based on the high amplitude noise of the freestream temperature and the consequent effect on the wall temperature evolution, the extraction of the heat transfer coefficient with polynomial fits results unfeasible. Additional attempts to improve the calculation of the heat transfer coefficient have been rejected due to its handicap to capture a realistic value during the blowdown.

In order to compute the heat transfer coefficient over reasonable test windows a set of criteria are defined. This procedure was automatically applied to all the tests. The criteria consists on

(a) test start, based on T_0 raise
(b) test end, based on T_0 sudden decay
(c) root-mean-square deviation $(T_0) < 2\%$ from down-sampled signal
(d) positive slope of the wall temperature
(e) negative slope of the heat flux
(f) minimum window size of 5 ms.

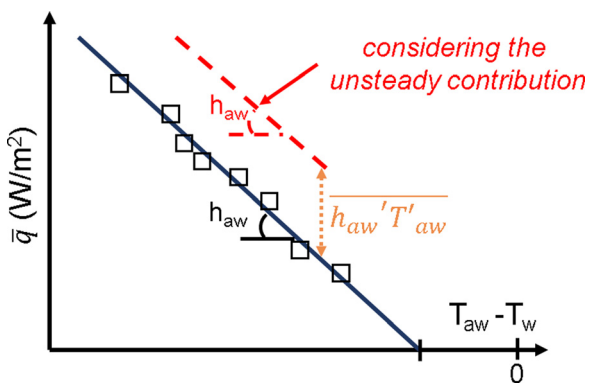

Fig. 6 Unsteady contribution of the heat transfer coefficient characterization

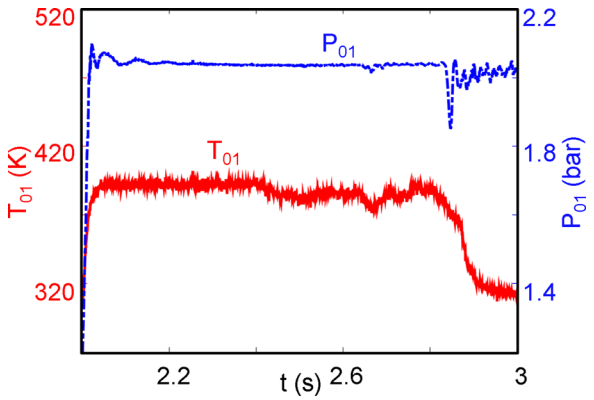

Fig. 7 Experimental total pressure and temperature

The application of the prescribed criteria is depicted in Fig. 9. The scattered windows show valid regions for the local graph whereas on the freestream total temperature evolution the solid lines depict the valid test duration. Finally, the temporal locations were all the criteria are met are selected as overall valid windows. In case there exist several windows during the same test, the wider one is selected, and the heat transfer coefficient is calculated over it.

4 Transonic Short Transient Application

4.1 Wind Tunnel. The transient isentropic compression tube facility of the von Karman Institute was used for the experimental investigation, designed for convective heat transfer research. The rig provides testing time up to 800 ms depending on the conditions to be replicated [31]. Such a transient offers a temperature gradient between the working fluid and the wall, essential for heat transfer measurements while accommodating sufficient duration for data acquisition. A lightweight piston driven with highly pressurized air at around 250 bar compresses dry-air inside the cylinder. The piston-pressurized air is suddenly released to the test section by a fast acting valve when the desired upstream total pressure and temperature are reached. Finally, the test air is vented to the atmosphere through an anechoic chamber in order to reduce the acoustic signature of the experiments (Figs. 10(*a*) and 10(*b*). The initial pressure in the compression tube can be selected to attain a wide range of upstream total pressures and temperatures matching engine representative Mach and Reynolds numbers [32,33].

Figure 10(*d*) depicts the test section that was designed to accommodate a linear cascade of two flow passages derived from a documented transonic HP stator [32] (Fig. 10(*e*)). The geometry was scaled up to increase spatial resolution of the measurements while mimicking the pressure distribution of the modern HP vanes. Moreover, the enlarged model was designed to maintain a

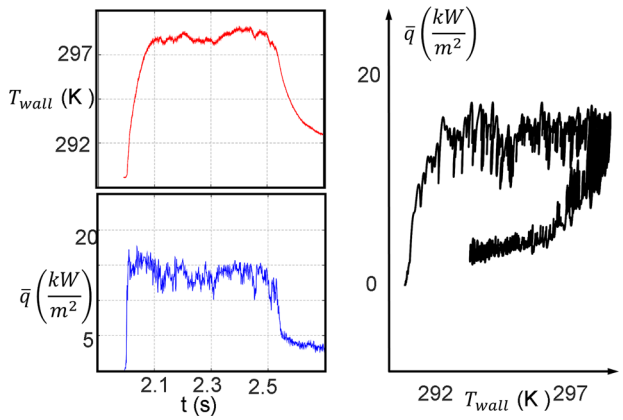

Fig. 8 Methodology application

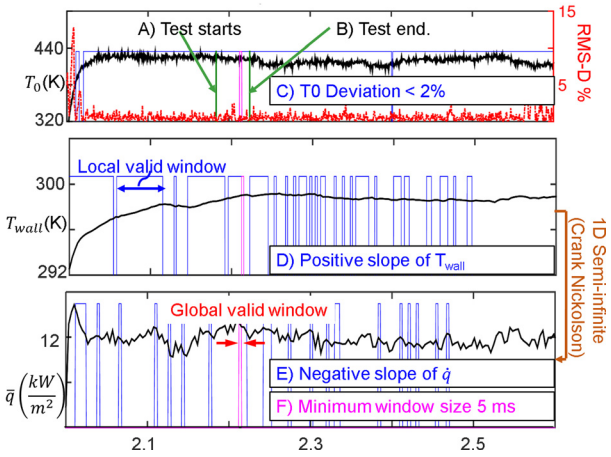

Fig. 9 Criteria application for test window definition

similar velocity distribution while reducing the trailing edge unsteadiness derived from the vortex shedding; thus, increasing the temporal resolution. The complete suction surface of the model was fitted by a high-order Bezier curve to ensure second-order continuous curvature, thus, a smooth velocity profile all along the airfoil. The pressure surface, on the other hand, was kept flat in order to have axial outlet flow required to accommodate the scaled up model. In both the turbine and test airfoil, the rear passage is identical, from the throat till the trailing edge. Therefore, in this transonic test case, the rear suction side is submitted to a Prandtl–Meyer expansion from the throat till the impact of the shock wave. In spite of the lower turning, the resulting static pressure distributions, in the turbine and test airfoils are the same.

A valve with a perforated rotating disk inside provided the pulses on the coolant stream. The outlet of the valve was connected to plenum of the model from an opening on the sidewall of the test section. A controlled gradual reduction on the cooling cavity cross section was imposed to avoid the flow blockage before the trailing edge of the model. The precision of the coolant plenum inside of the model was achieved through a single piece laser sintering method manufacture. The flow field upstream and downstream of the cooling system including the rotating valve, connection piping, and the model was modeled in detail prior to the wind tunnel experiments [34].

The experimental conditions encompasses Mach numbers ranging from high subsonic to low supersonic ($M_{2,is} = 0.8$–1.2) and two engine representative Reynolds numbers ($Re = 4 \times 10^6$ and 6×10^6). The tests were conducted for continuous purge of coolant as well as uncooled baseline. The pulsating coolant flow was admitted at average coolant total pressure of 1.9 bars with a frequency of 200 Hz.

4.2 Effect of Trailing Edge Blowing. The aforementioned methodology was applied to the experimental results in the linear transonic cascade. Figure 11 represents the heat transfer coefficient evolution on two airfoil locations for two freestream conditions with three diverse blowing schemes. There exists a noticeable difference on the heat transfer levels on both Mach number experiments. The main reason is the transition from laminar to turbulent boundary layer. At the lowest Mach number, the boundary layer remains laminar through the entire airfoil suction side. Whereas, the shock wave boundary layer interaction ignites the transition to turbulent boundary layer at the highest Mach number [35–37]. The heat flux propagation through a turbulent boundary layer is favored due to the enhanced mixing with turbulence. Consequently, the heat transfer coefficient results larger for the higher Mach number.

Due to the uniform boundary layer growth in the subsonic case, the boundary layer over the downstream gage is thicker providing more isolating flow, reflected in a lower heat transfer coefficient.

In the supersonic outlet condition, a raise on the heat transfer coefficient with the cooling ejection is noticed. This is the effect of the separation bubble generated at the impingement of the

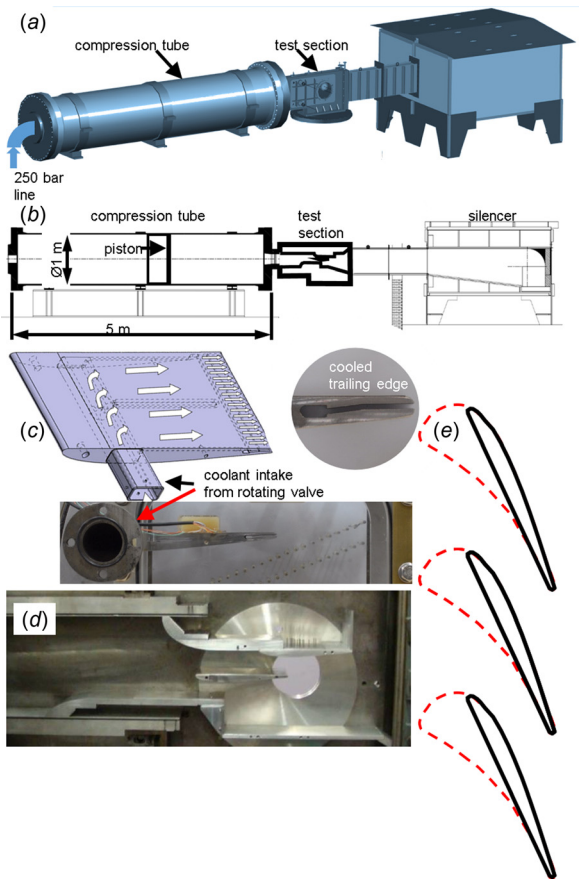

Fig. 10 (*a*) and (*b*) Blow down facility at von Karman Institute, (*c*) turbine airfoil cooling distribution, (*d*) test section, and (*e*) test airfoil

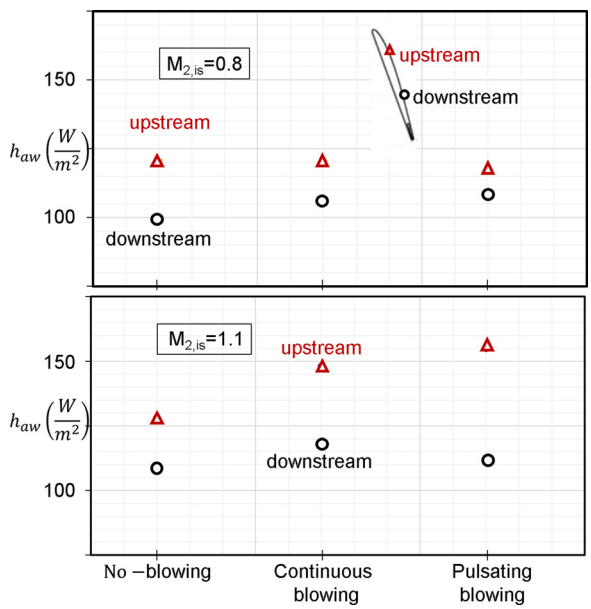

Fig. 11 Trailing blowing ratio effect on the heat transfer coefficient distribution

shock wave. The bubble is a recirculation region where the flows from boundary layer and the shock wave interact and form vortical structures, which then enhances heat transfer from the flow to the wall. Consequently, the heat transfer coefficient is augmented due to the presence of the recirculation bubble, as described by Gifford et al. [38]. Saracoglu et al. [11] exposed how for higher cooling pressures the shock impingement is displaced upstream, getting closer to the passage throat. Similarly, with pulsating blowing conditions the shock is further shifted upstream.

The flow constantly increases its speed over the suction surface over accelerates owing the Prandtl–Meyer expansion fan, and then suddenly decelerates though the trailing edge shock wave impingement. Downstream of the impingement location, the boundary layer reattaches and continues to accelerate until the trailing edge region. Figure 12 Schlieren photograph and numerical Schlieren, both reveal the same flow topology. Illustrating the lip-shocks emanating from the trailing edge, as well and the main shock from the wave, and then impinging on the rear suction side

Johnson et al. [39], presented a summary of the main researches done in the topic of the shock wave boundary layer interaction at both laminar and turbulent conditions. The experimental results obtained by Herbert Law [40] documents recirculation bubble geometrical scale for several Reynolds numbers as a function of the obstacle angle and boundary layer thickness. Based on the prior literature, the size of the shock boundary layer interaction bubble can reach at least up to three boundary layer thicknesses upstream [37, 41–43].

Based on the estimation of the bubble factor and the boundary layer thickness, the propagation of the shock impingement bubble can be addressed. Based on the computation fluid dynamics results [11], the boundary layer thickness is around 2 mm, which means that the bubble itself could arrive 6 mm upstream of the shock impingement. The existence of the bubble is propagated further upstream since the boundary layer needs to accommodate its height to the downstream perturbations. The region of the upstream gauge is already affected by the existence of the recirculation region as a consequence of the shock impingement.

4.3 Uncertainty Evaluation. In order to quantify the uncertainty of the heat transfer measurements several factors must be taken into account. The main sources of uncertainty in the methodology are the wall temperature acquisition, the heat flux processing, and the procedure to obtain the adiabatic wall temperature and the adiabatic heat transfer coefficient. All error evaluations are given at 95% confidence level.

The wall temperature measurement is provided by the thin-film gauges acting as resistance thermometers through the acquisition boxes. Errors may be induced during the calibration on the reference temperature (T_{01}) and the resistivity coefficient α_T, based on Eq. (1). Additionally, the experimental noise creates random uncertainty in the acquisition procedure. During the post processing, the main cause of errors could be based on the mismatching of the material properties, thickness, conductivity (κ), or density (ρ). The bottom layer material properties mismatch effect results negligible compared with the first layer. The uncertainty in the heat transfer quantification is due to several factors: the number of experimental data in the windowed range, the wall temperature range, the thin film data acquisition, and heat flux computation procedure.

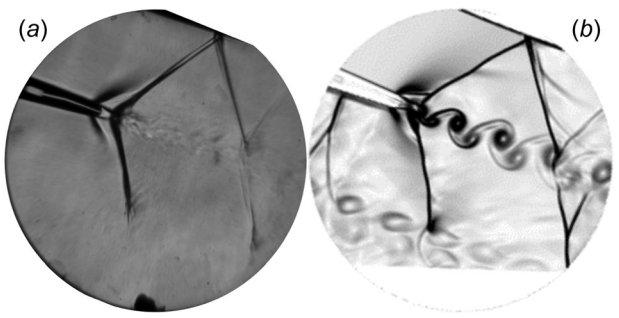

Fig. 12 Experimental (*a*) and numerical (*b*) Schlieren images of the test section at Mach 1.1 [7]

Table 2 Heat flux uncertainty

	Value	Unit	Uncertainty	Sensitivity
Upilex thickness	0.15	mm	15×10^{-4}	83.70
Upilex, κ	0.29	W/m/K	0.011	76.02
Upilex, ρ	1470	kg/m^3	58.8	11.76
Aluminum thickness	0.04	mm	2×10^{-4}	0.00
Aluminum κ	180	W/m/K	7.2	4.11
Aluminum ρ	2700	kg/m^3	108	0.86
T_w	333	kg/m^3	1.66	28.47
$\overline{q}$ @ $t = 0.3$ s	37 kW/m^2		Global $\Delta\,\overline{q}$	3.2%

Table 3 Heat transfer coefficient uncertainty

	Value	Unit	Uncertainty	Sensitivity
Upilex thickness	0.15	mm	15×10^{-4}	2265
Upilex κ	0.29	W/m/K	0.011	435.2
Upilex ρ	1470	kg/m^3	58.8	356.1
Aluminum thickness	0.04	mm	2×10^{-4}	0.00
Aluminum κ	180	W/m/K	7.2	34.6
Aluminum ρ	2700	kg/m^3	108	34.3
T_w	333	kg/m^3	1.66	37.6
h_{aw}	202 W/(m^{2}K)		Global Δh_{aw}	32%

Possible anisotropic characteristics of the airfoil material would result in a multidimensional heat flux and higher uncertainty. Additional white noise must be considered from the conditioning electronics and the resistance foil. The uncertainty analysis derived from the material properties is presented in Table 2, as described by Moffat [44]. Based on the uncertainty of the material properties and wall temperature, the global uncertainty on the heat flux is 3%.

Similarly, Table 3 presents the input data required to assess the uncertainty in the convective heat transfer coefficient. The fourth column lists the uncertainty due to each contribution, while the fifth shows the sensitivity. The upilex layer properties play a dominant role in the uncertainty. In the present experiments, the overall uncertainty, obtained as root-mean-square of all the uncertainties, equals 32%.

5 Conclusions

An experimental study of a transonic linear cascade with trailing edge cooling has been completed. The effect of several cooling conditions ranging from null to continuous or pulsating coolant ejection on the heat flux distribution over the airfoil have been experimentally investigated. The tests were carried out at realistic Mach numbers for high pressure turbines (0.8, 1.1), and representative Reynolds numbers. The detrimental effects of the trailing edge shock waves on the neighboring airfoil and downstream plane are reduced with coolant ejection. The heat transfer distribution along the suction side of a transonic high-pressure turbine has been analyzed based on high frequency thin film wall temperature measurements. Providing an insight of the trailing edge cooling effects of the heat flux distribution for the next generation of turbine designs. An innovative methodology has been presented to postprocess thin film measurements based on a single experiment making use of the adiabatic wall temperature definition.

Acknowledgment

The authors would like to acknowledge the financial support of U.S. Air Force under the frame of the Project AFOSR FA 8655-

08-1-3033. The authors also wish to thank the support of Tolga Yasa, Simone Duni, Marcos Gonzalez, and Dominick Christoffels from von Karman Institute for Fluid Dynamics.

Nomenclature

c_{ax} = axial cord (m)
h = heat transfer coefficient (W/(m^{2}K))
M = Mach, u/c
P = pressure (bar)
Pr = Prandtl number
q = heat flux (W)
R = resistance
Re = Reynolds, $\rho c_{ax} V_2/\mu$
TE = trailing edge
T = temperature (K)
V = velocity (m/s)

Greek Symbols

κ = thermal conductivity(W/(m K))
μ = viscosity ((kg/(ms)))
ρ = density (kg/(m^3))
σ = recovery factor

Subscripts

alu = aluminum
aw = adiabatic wall
is = isentropic
r = relative
rec = recovery
up = Upilex
w = wall
0 = total conditions
1 = vane upstream conditions
2 = vane downstream conditions

References

[1] Paniagua, G., Yasa, T., de la Loma, A., Castillion, L., and Coton, T., 2008, "Unsteady Strong Shock Interactions in a Transonic Turbine: Experimental and Numerical Analysis," J. Propul. Power, **24**(4), pp. 722–731.
[2] Denton, J. D., and Xu, L., 1990, "The Trailing Edge Loss of Transonic Turbine Blades," ASME J. Turbomach., **112**(2), pp. 277–285.
[3] Denton, J. D., 1993, "Loss Mechanisms in Turbomachinery," ASME J. Turbomach., **115**(4), pp. 621–656.
[4] Motallebi, F., and Norbury, J. F., 1981, "The Effect of Base Bleed on Vortex Shedding and Base Pressure in Compressible Flow," J. Fluid Mech., **110**, pp. 273–292.
[5] Kapteijn, C., Amecke, J., and Michalassi, V., 1996, "Aerodynamic Performance of a Transonic Turbine Guide Vane With Trailing Edge Coolant Ejection: Part I—Experimental Approach," ASME J. Turbomach., **118**(3), pp. 519–528.
[6] Raffel, M., and Kost, F., 1998, "Investigation of Aerodynamic Effects of Coolant Ejection at the Trailing Edge of a Turbine Blade Model by PIV and Pressure Measurements," Exp. Fluids, **24**(5), pp. 447–461.
[7] Saracoglu, B. H., Paniagua, G., Sanchez, J., and Rambaud, P., 2013, "Effects of Blunt Trailing Edge Flow Discharge in Supersonic Regime," Comput. Fluids, **88**, pp. 200–209.
[8] Andrews, S. A., Mahallati, A., Allan, W. D., and Benner, M. W., 2009, "Experimental and Computational Investigation of the Mid-Span Flowfield in a Transonic Turbine Nozzle Cascade," 19th International Symposium on Airbreathing Engines, Montreal, Canada, Sept. 7–11, Paper No. ISABE-2009-123.
[9] Sieverding, C. H., Stanislas, M., and Snoeck, J., 1980, "The Base Pressure Problem in Transonic Turbine Cascades," ASME J. Eng. Power, **102**(3), pp. 711–718.
[10] Sieverding, C. H., 1983, "The Influence of Trailing Edge Ejection on the Base Pressure in Transonic Turbine Cascades," ASME J. Eng. Power, **105**(2), pp. 215–222.
[11] Saracoglu, B. H., Paniagua, G., Salvadori, S., Tomasoni, F., Duni, S., Yasa, T., and Miranda, A., 2012, "Trailing Edge Shock Modulation by Pulsating Coolant Ejection," Appl. Therm. Eng., **48**, pp. 1–10.
[12] Dunn, M. G., and Stoddard, F. J., 1977, *Studies of Heat Transfer to Gas Turbine Components*, Calspan, Buffalo, NY, pp. 1–48.
[13] Nicholson, J. H., Forest, A. E., Oldfield, M. L. G., and Schultz, D. L., 1984, "Heat Transfer Optimized Turbine Rotor Blades—An Experimental Study Using Transient Techniques," ASME J. Eng. Gas Turbines Power, **106**(1), pp. 173–182.
[14] Arts, T., and Lambert de Rouvroit, L., 1992, "Aero-Thermal Performance of a Two-Dimensional Highly Loaded Transonic Turbine Nozzle Guide Vane: A Test Case for Inviscid and Viscous Flow Computations," ASME J. Turbomach., **114**(1), pp. 147–154.
[15] Dunn, M. G., 1986, "Heat-Flux Measurements for the Rotor of a Full-Stage Turbine: Part I—Time-Averaged Results," ASME J. Turbomach., **108**(1), pp. 90–97.
[16] Moffat, R. J., 1998, "What's New in Convective Heat Transfer?," Int. J. Heat Fluid Flow, **19**(2), pp. 90–101.
[17] Collins, M., Chana, K., and Povey, T., 2015, "Improved Methodologies for Time Resolved Heat Transfer Measurements, Demonstrated on an Unshrouded Transonic Turbine Casing," ASME Paper No. TURBO-16-1051.
[18] Pinilla, V., Solano, J. P., Paniagua, G., and Anthony, R. J., 2012, "Adiabatic Wall Temperature Evaluation in a High Speed Turbine," ASME J. Heat Transfer, **134**(9), p. 091601.
[19] Doorly, J. E., Oldfield, M. L. G., and Jones, T. V., 1973, "The Theory of Advanced Multi-Layer Thin Film Heat Transfer Gauges," Int. J. Heat Mass Transfer, **30**(6), pp. 1159–1168.
[20] Doorly, J. E., and Oldfield, M. L. G., 1986, "New Heat Transfer Gauges for Use on Multilayered Substrates," ASME J. Turbomach., **108**(1), pp. 153–160.
[21] Oldfield, M. L. G., 2008, "Impulse Response Processing of Heat Transfer Gauge Signals," ASME J. Turbomach., **130**(2), p. 021023.
[22] Iliopoulou, V., Denos, R., Billiard, N., and Arts, T., 2004, "Time-Averaged and Time-Resolved Heat Flux Measurements on a Turbine Stator Blade Using Two-Layered Thin-Film Gauges," ASME J. Turbomach., **126**(4), pp. 570–577.
[23] Schultz, L. D., and Jones, T. V., 1973 "Heat Transfer Measurements in Short Duration Facilities," AGARDograph Report, Report No. 165.
[24] Billard, N., Iliopoulou, V. F., and Denos, R., 2002 "Data Reduction and Thermal Product Determination for Single and Multi-Layered Substrates Thin-Film Gauges," 16th Symposium on Measuring Techniques, Cambridge, UK, Sept., Paper No. 6–2.
[25] Crank, J., and Nicolson, E., 1996, "A Practical Method for Numerical Evaluation of Solutions of Partial Differential Equations of the Heat-Conduction Type," Adv. Comput. Math., **6**(1), pp. 207–226.
[26] Bergman, T. L., Lavine, A. S., Incropera, F. P., and Dewitt, D. P., 2002, *Fundamentals of Heat and Mass Transfer*, 7th ed., Wiley, New York.
[27] Popp, O., Smith, D. E., Bubb, J. V., Grabowski, H. C., III, Diller, T. E., Schetz, J. A., and Ng, T. E., 2000, "Investigation of Heat Transfer in a Film Cooled Transonic Turbine Cascade, Part I: Steady Heat Transfer," ASME Paper No. 2000-GT-0202.
[28] Lavagnoli, S., De Maesschalck, C., and Paniagua, G., 2014, "Uncertainty Analysis of Adiabatic Wall Temperature Measurements in Turbine Experiments," Appl. Therm. Eng., **82**, pp. 170–181.
[29] Guo, S. M., Spencer, M. C., Lock, G. D., Jones, T. V., and Harvey, N. W., 1995, "The Application of Thin Film Gauges on Flexible Plastic Substrates to the Gas Turbine Situation," ASME Paper No. 95-GT-357.
[30] Thorpe, S. J., Yoshino, S., Ainsworth, R. W., and Harvey, N. W., 2004, "Improved Fast-Response Heat Transfer Instrumentation for Short-Duration Wind Tunnels," Meas. Sci. Technol., **15**(9), pp. 1897–1909.
[31] Shultz, D. L., Jones, T. V., Oldfield, M. L. G., and Daniels, L. C., 1978, "A New Transient Facility for the Measurement of Heat Transfer Rates in High Temperature Problems in Gas Turbine Engines," AGARD CP 229, Paper No. 28.
[32] Sieverding, C. H., Arts, T., Dénos, R., and Martelli, F., 1996, "Investigation of the Flow Field Downstream of a Turbine Trailing Edge Cooled Nozzle Guide Vane," ASME J. Turbomach., **118**(2), pp. 291–300.
[33] Jones, T. V., Shultz, D. L., and Hendley, A. D., 1973, "On the Flow in an Isentropic Free Piston Tunnel," ARC R&M 3731.
[34] Gonzalez, M., Paniagua, G., Saracoglu, B., and Tiseira, A., 2010, "Pulsating Cooling System for High-Pressure Turbine Blades," AIAA Paper No. 2010-4587.
[35] Dolling, D. S., 2001, "Fifty Years of Shock Wave Boundary Layer Interaction Research: What's Next?," AIAA J., **39**(8), pp. 1517–1531.
[36] D'Ambrosio, D., 2002, "A Study on Shock Wave-Boundary Layer Interactions in High-Speed Flows," 4th European Symposium Aerothermodynamics for Space Vehicles, Capua, Italy, Oct. 15–18, pp. 733–742.
[37] Dupont, P., Haddad, C., and Debieve, J. F., 2006, "Space and Time Organization in a Shock-Induced Separated Boundary Layer," J. Fluid Mech., **559**, pp. 255–277.
[38] Gifford, A. R., Diller, T. E., and Vlachos, P. P., 2011, "The Physical Mechanism of Heat Transfer Augmentation in Stagnating Flows Subject to Freestream Turbulence," ASME J. Heat Transfer, **133**(2), p. 021901.
[39] Johnson, A. B., Rigby, M. J., and Oldfield, M. L. G., 1989, "Unsteady Aerodynamic Phenomena in a Simulated Wake and Shock Wave Passing Experiment," AGARD, Paper No. CP-468.
[40] Herbert Law, C., 1976, "Supersonic Shock Wave Turbulent Boundary Layer Interactions," AIAA J., **14**(6), pp. 730–734.
[41] Humble, R. A., Scarano, F. B., and van Oudhesden, W., 2007, "Unsteady Flow Organization of a Shock wave/Turbulent Boundary Layer Interaction," Exp. Fluids, **43**, pp. 173–183.
[42] Horstman, C. C., Settles, G. S., Vas, I. E., Bogdonoff, S. M., and Hung, C. M., 1977, "Reynolds Number Effects on Shock-Wave Turbulent Boudnary-Layer Interaction," AIAA J., **15**(8), pp. 1152–1158.
[43] Katzer, E., 1988, "On the Length Scales of Laminar Shock/Boundary Layer Interaction," J. Fluid Mech., **206**, pp. 477–496.
[44] Moffat, R. J., 1988, "Describing the Uncertainties in Experimental Results," Exp. Therm. Fluid Sci., **1**(1), pp. 3–17.